Properties of MOCVD Deposits Using Novel Sn(II) Neo-Pentoxide Precursors

Timothy J. Boyle,*,† Timothy L. Ward,‡ Sacha M. De'Angeli,† Huifang Xu,§ and William F. Hammetter†

Advanced Materials Laboratory, Sandia National Laboratories, 1001 University Boulevard SE, Albuquerque, New Mexico 87106, and Departments of Chemical and Nuclear Engineering and Earth and Planetary Sciences, University of New Mexico, Albuquerque, New Mexico 87131

Received September 5, 2002

A family of Sn(II) oxo-alkoxy precursors were investigated for MOCVD applications, which included $[Sn(\mu\text{-}ONep)_2]_\infty$ (**1**, ONep = OCH_2CMe_3) and its hydrolysis products $[Sn_5(\mu_3\text{-}O)_2(\mu\text{-}ONep)_6]$ (**2**) and $[Sn_6(\mu\text{-}O)_4(ONep)_4]$ (**3**). Each was found to possess high enough volatility at low temperatures, as indicated by melting point and TGA/DTA data, to warrant investigation as MOCVD precursors to tin oxide thin films. The experimental setup used a lamp-heated cold-wall CVD reactor with direct vaporization of the precursor, without a carrier gas. Compounds **1**−**3** failed to produce uniform films, but powders and wires of tin oxide and Sn metal were formed under the appropriate conditions. The resultant deposits on Si wafers were investigated using SEM, XRD, and TEM techniques. The nonhydrolyzed species **1** preferentially formed spheres of Sn^0 whereas the partially hydrolyzed species **2** formed wires of tin oxide from a proposed vapor−liquid−solid mechanism using Sn^0 as the seed. Compound **3** formed an intermediate species possibly due to its more condensed nature limiting its volatility. In general, these compounds are useful for MOCVD, but other conditions or deposition techniques are necessary to form high-quality thin films of tin oxide.

Introduction

We previously reported on the utility of group IV *neo*-pentoxide (ONep = OCH_2CMe_3) compounds as acceptable metal−organic chemical vapor deposition (MOCVD) precursors for the production of ceramic thin films. The ONep derivatives of Ti and Zr were found to produce high-quality films of anatase and zirconium oxide, respectively, at relatively low temperatures.[1] Other attractive characteristics of these derivatives were their low vaporization temperatures, low deposition temperatures, and a "clean" decomposition pathway that yielded high-purity thin films with low carbon contamination. $[Ti(\mu\text{-}ONep)(ONep)_3]_2$ was especially useful since it is a powder but possesses a very low melting point so that it acts much like an oil. Oils are useful in CVD applications due to their continuous vaporization rates but typically these precursors are very susceptible to continual hydrolysis. In contrast, powders react to a lesser extent but typically possess too low a volatility to make them feasible CVD precursors. Therefore, powders with low melting points coupled with high volatility and low decomposition temperatures are of interest.

Tin oxide (SnO_x) thin films have a wide range of varied applications such as gas sensors (NO_x, CO_x, HOR, CH_4),[2−11] solar cells,[12,13] reversible thermoelectric converters,[14] phosphors,[15] and anodes of Li^+ batteries.[16−18] While several reports exist on Sn precursors bearing oxygen-containing ligands for the production of SnO_x thin films,[19−21] only recently have these reports detailed

* To whom correspondence should be addressed. E-mail: tjboyle@Sandia.gov.
† Sandia National Laboratories.
‡ Department of Chemical and Nuclear Engineering, University of New Mexico.
§ Department of Earth and Planetary Sciences, University of New Mexico.

(1) Gallegos, J. J. I.; Ward, T. L.; Boyle, T. J.; Francisco, L. P.; Rodriguez, M. A. *Adv. Mater. CVD* **2000**, *6*, 21.
(2) Koh, S. K.; Jung, H. J.; Song, S. K.; Choi, W. K.; Choi, D.; Jeon, J. S. U.S. Patent 6059937, 2000.
(3) Chou, J. C.; Chung, W.-Y.; Hsiung, S.-K.; Sun, T.-P.; Liao, H.-K. U.S. Patent 6218208, 2001.
(4) Koh, S. K.; Jung, H. J.; Song, S. K.; Choi, W. K.; Choi, D.; Jeon, J. S. U.S. Patent 5989990, 1999.
(5) Chang, S.-C. U.S. Patent 4169369, 1979.
(6) Abbas, M. N.; Moustafa, G. A.; Gopel, T. V. *Anal. Chim. Acta* **2001**, *4331*, 181.
(7) Chaudhary, B. A.; Mulla, I. S.; Vijayamohanan, K.; Hegde, S. G.; Srinivas, D. *J. Phys. Chem. B* **2001**, *105*, 2565.
(8) Gregory, O. J.; Luo, Q. *Sens. Actuators, A* **2001**, *88*, 234.
(9) Hellegouarc'h, F.; Arefi-Khonsari, F.; Planade, R.; Amouroux, J. *Sens. Actuators B* **2001**, *73*, 27.
(10) Tarabek, J.; Wolter, M.; Rapta, P.; Plieth, W.; Maumy, M.; Dunsch, L. *Macromol. Symp.* **2001**, *164*, 219.
(11) Yoshimi, Y.; Ohdira, R.; Iiyama, C.; Sakai, K. *Sens. Actuators B* **2001**, *73*, 49.
(12) Amin, N.; Isaka, T.; Yamada, A.; Konagai, M. *Sol. Energy Mater. Sol. Cells* **2001**, *67*, 195.
(13) Veluchamy, P.; Tsuji, M.; Nishio, T.; Aramoto, T.; Higuchi, H.; Kumazawa, S.; Shibutani, S.; Nakajima, J.; Arita, T.; Ohyama, H. *Sol. Energy Mater. Sol. Cells* **2001**, *67*, 179.
(14) Yater, J. C.; Yater, J. A.; Yater, J. E. U.S. Patent 5889287, 1999.
(15) Chadha, S. S.; Alwan, J. J. U.S. Patent 5695809, 1997.
(16) Mohamedi, M.; Lee, S. J.; Takahashi, D.; Nishizawa, M.; Itoh, T.; Uchida, I. *Electrochim. Acta* **2001**, *46*, 1161.
(17) Nam, S. C.; Yoon, Y. S.; Cho, W. I.; Cho, B. W.; Chun, H. S.; Yun, K. S. *Electrochem. Commun.* **2001**, *3*, 6.
(18) Nam, S. C.; Yoon, Y. S.; Cho, W. I.; Cho, B. W.; Chun, H. S.; Yun, K. S. *J. Electrochem. Soc.* **2001**, *148*, A220.
(19) Kane, J.; Schweizer, H. P.; Kern, W. *J. Electrochem. Soc.* **1975**, *122*, 1144.

10.1021/cm020893p CCC: $25.00 © 2003 American Chemical Society
Published on Web 01/14/2003

Table 1. A Metrical Comparison of Properties of Selected SnO_x MOCVD Precursors[a]

precursor	T_b (°C)	T_d (°C)	dep. rate (nm/min)	dep. *P* (Torr) (carrier gas)	impurities	ref
$Sn(OC(CH_3)_3)_4$	80	250−400	≈25	760 (N_2)	<0.2% C	23, 24
	45		≈42	15 (N_2)		
$Sn(OCH(CF_3)_2)_4(HN(CH_3)_2)$	110−120	200−450	100	0.45 (air)	<3% C	22
			0	(dry O_2)	F/Sn < 0.026	
$Sn(OCH(CF_3)_2)_2(HN(CH_3)_2)$	90−100	180−450	26−58	0.45 (air)	<5% C	22
			390−700	0.1 (H_2O)	F/Sn = 0.1−0.4	
			0	(dry)		
$Sn(acac)_2$	50−150	100−600	0	760 (N_2)	nr	20
			0.1−100	760 (air)		
$Sn(O_2CCF_3)_2$	140−160	250−500	0	760 (N_2)	F/Sn = 0.027	21
			21 (400 °C)	760 (O_2/N_2)		
$Sn(O_2CCH_3)_2$	120−160	200−500	0	760 (N_2)	nr	21
			5−50	760 (O_2/N_2)		
$(C_4H_9)_2Sn(O_2C_2H_3)_2$	70−150	420	7−24	760 (O_2/H_2O in N_2)	nr	19

[a] T_b = bubbler or vaporization temperature. T_d = deposition temperature. nr = not reported.

the utility of metal alkoxide precursors for the MOCVD production of SnO_x thin films: $Sn(OCH(CF_3)_2)_4(HNMe_2)_2$[22] and $Sn(OCMe_3)_4$.[23,24] The fluorinated species yielded halide-doped films, which are of interest for high-conductivity applications, but may be problematic for other applications. The $OCMe_3$ species proved to be a viable means for production of SnO_2 thin films without the use of an oxidant; however, this Sn(IV) precursor necessitated the use of a carrier gas to generate the films.[23,24] Table 1 shows some of the properties reported for oxygen-bearing Sn MOCVD precursors.

Recently, we reported the synthesis of $[Sn(ONep)_2]_\infty$ (**1**) and two of its condensation products $[Sn_5(\mu_3{-}O)_2(\mu\text{-}ONep)_6]$ (**2**) and $[Sn_6(\mu\text{-}O)_4(ONep)_4]$ (**3**) (see Figure 1).[25] On the basis of the continued interest in SnO_x thin films, the physical properties of **1**−**3**, the need for alternative precursors for MOCVD, and the potential differences that may be observed with these precursors, we investigated the utility of these compounds as potential MOCVD reagents. The experimental conditions and the resultant depositions are presented and compared to those precursors currently in use.

Experimental Section

All precursors were handled under an inert atmosphere. $[Sn(ONep)_2]_\infty$ (**1**), $[Sn_5(\mu_3{-}O)_2(\mu\text{-}ONep)_6]$ (**2**), and $[Sn_6(\mu\text{-}O)_4(ONep)_4]$ (**3**) were prepared according to the literature report.[25] A full summary of the conditions that were used are presented in Table 2 and a schematic of the CVD benchtop reactor was previously reported.[1]

Thermogravimetric analysis/differential thermal analysis (TGA/DTA) data were collected on a TA Instruments STD 2960 simultaneous TGA/DTA. Si(100) (native oxide surface) substrates were cleaved into ≈1-cm^2 pieces prior to use. The X-ray diffraction (XRD) data on the samples were collected using a zero background holder on a Siemens D500 $\theta{-}\theta$ diffractometer (10−80 θ range, 0.02 step size, and a 5-s count time) equipped with Cu Kα radiation, a graphite monochromator, and a scintillation detector, and data were refined using the JADE software package (Materials Data Inc., Livermore, CA). Scanning electron microscopy (SEM) was conducted on gold-sputtered samples and images collected on an Amray 1830 scanning electron microscope. X-ray photoelectron spectroscopy (XPS) data were collected on a Kratos Analytical AXIS-His instrument. Transmission electron microscopy was carried out using a JEOL 2010 HREM equipped with Oxford-Link X-ray energy-dispersive spectroscopy (EDS). A GATAN slow scan CCD camera was used for recording TEM images and electron diffraction patterns.

An outline of the general methodology that was used for the production of the deposits follows: (i) under an argon atmosphere, the precursor (≈0.5 g) was placed in a straight flask equipped with a Teflon stopcock and O-ring adapter (delivery flask) and sealed; (ii) the delivery flask was connected to the reactor and placed under vacuum; (iii) the reactor walls were heated by heating tape to ≈10 °C above the vaporization temperature; (iv) the substrate was heated to deposition temperature by a heating lamp and the deposition temperature was sensed by a thermocouple in direct contact with the substrate and controlled by an Omega CN9000 controller and a variable autotransformer (Variac); (v) the precursor pot was heated to the vaporization temperature by heating tape and the precursor pot temperature was sensed by a thermocouple in contact with the outside of the pot and controlled by an Omega CN9000 controller and Variac; (vi) once the pressure and temperatures were all stable, the delivery flask stopcock was opened to the reactor, and the experiment was carried out until the precursor was vaporized (signaled by a significant drop in reactor pressure); (vii) all experiments were terminated by closing the stopcock before turning off power to the heating tapes and heating lamp and by maintaining a vacuum until the substrate temperature dropped below 100 °C.

Results

Figure 1 shows the thermal ellipsoid plot of $[Sn(\mu\text{-}ONep)_2]_\infty$ (**1**), which can be stoichiometrically reacted with H_2O to form either $[Sn_5(\mu_3{-}O)_2(\mu\text{-}ONep)_6]$ (**2**) or $[Sn_6(\mu\text{-}O)_4(ONep)_4]$ (**3**). Compound **2** could also be converted to **3** through additional hydrolysis. These compounds were found to be soluble in a wide range of solvents and displayed high volatility by subliming intact (**1**, 150 °C; **2**, 170 °C; **3**, 170 °C at 10^{-4} Torr). A melting point determination revealed that **1** melts at ≈147 °C, **2** at ≈119 °C, and **3** at ≈185 °C under argon at atmospheric pressure.

Additional thermal investigations using TGA/DTA (argon at atmospheric pressure, Figure 2) revealed that initiation of ligand decomposition of this family of compounds under argon occurs around 120 °C (**1**), 150 °C (**2**), and 100 °C (**3**). For both **1** and **2**, almost full (≈75% and ≈85%, respectively) weight loss occurred, which is substantially greater than conversion to an oxide (i.e., material sublimes). Compound **3** lost ≈25%

(20) Maruyama, T.; Ikuta, Y. *Sol. Energy Mater. Sol. Cells* **1992**, *28*, 209.
(21) Maruyama, T.; Tabata, K. *J. Appl. Phys.* **1990**, *68*, 4282.
(22) Suh, S.; Hoffman, D. M.; Atagi, L. M.; Smith, D. C.; Liu, J.-R.; Chu, W.-K. *Chem. Mater.* **1997**, *9*, 730.
(23) Houlton, D. J.; Jones, A. C.; Hycock, P. W.; Williams, E. W.; Bull, J.; Critchlow, G. W. *Chem. Vap. Deposition* **1995**, *1*, 26.
(24) Brown, J. R.; Cheney, M. T.; Hycock, P.; Houlton, D. J.; Jones, A. C.; Williams, E. W. *J. Electrochem. Soc.* **1997**, *144*, 295.
(25) Boyle, T. J.; Alam, T. M.; Rodriguez, M. A.; Zechmann, C. A. *Inorg. Chem.* **2002**, *41*, 25742.

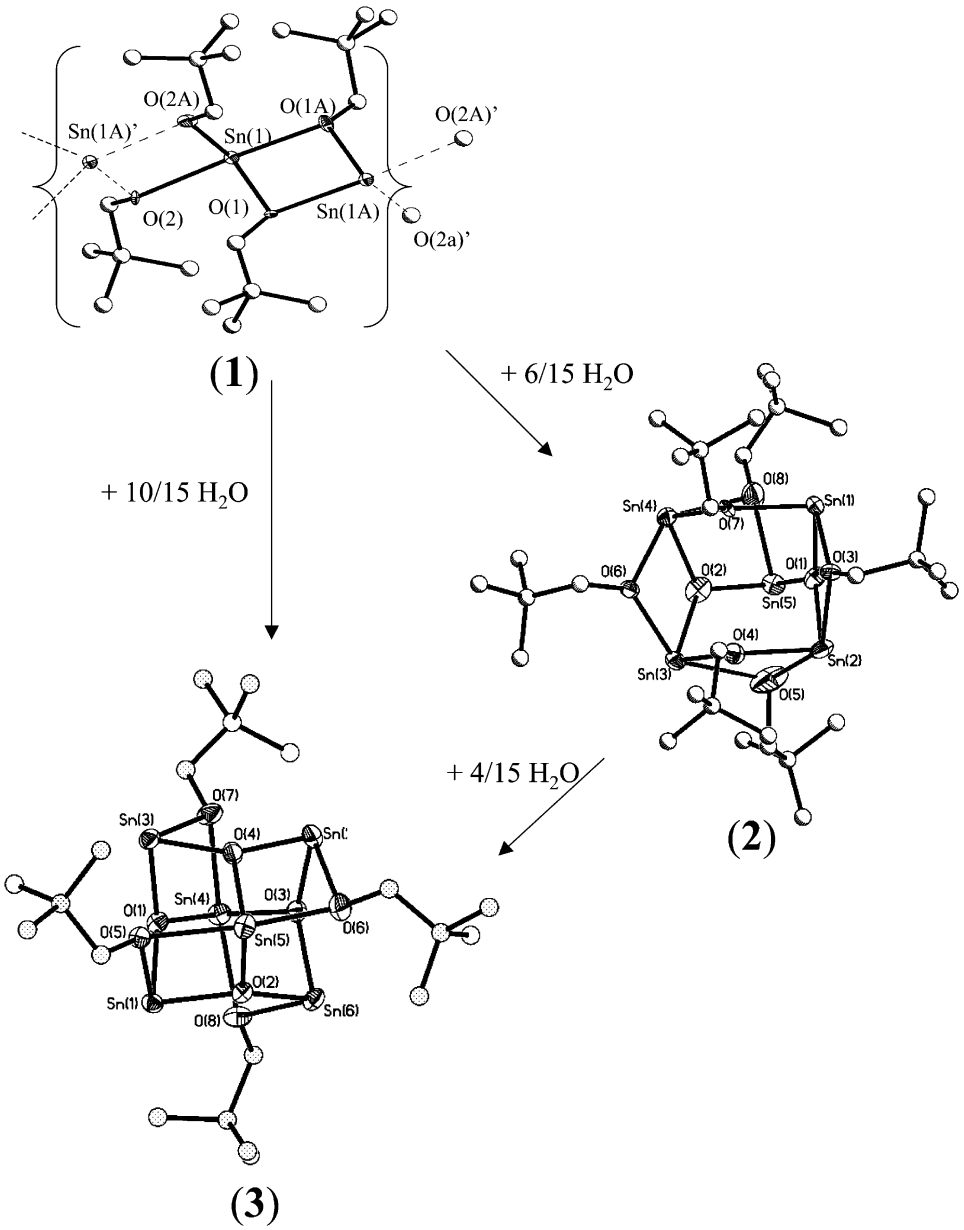

Figure 1. Thermal ellipsoid plot of the structure of $[Sn(\mu\text{-}ONep)_2]_\infty$ (**1**), $Sn_5(O)(ONep)$ (**2**), and $Sn_6(O)_4(ONep)_4$ (**3**) showing the chemical interconnections between these molecules.

Table 2. Typical Conditions Used To Deposit MO_2 Films from Compounds 1−3

variable	1	2	3
sample size (g)	0.2	0.2	0.2
reactor base pressure (mTorr)	75−85	75−85	75−85
deposition pressure (mTorr)	95−120	95−120	95−120
vaporization temperature (°C)	130	173	178
deposition temperature (°C)	315−500+	330−500+	350−440
substrates	Si(100)	Si(100)	Si(100)

of its original weight, which is more representative of conversion to the oxides. Compound **1** displayed a single weight loss over a relatively short range of temperature (160−190 °C) whereas **2** showed a broader (150 to 290 °C) two-step weight loss in a 1:1 ratio. Compound **3** revealed a three-step decomposition wherein the ratio of the weight loss in the first step to that in the second and third steps was approximately 1:1:2.

For each sample, films were generated as described in the Experimental Section at a variety of temperatures (10 °C intervals). All deposits were slightly gray in appearance, and for the majority of the deposits, simple wiping of the substrate would remove the deposit. XPS analysis of deposits from **1**−**3** indicated >20 at. % carbon in deposits over the 315−430 °C deposition temperature range. For each of the depositions generated by **1**−**3**, XRD, SEM, and TEM analyses were undertaken to characterize the final films.

Compound 1. XRD analyses of the resultant deposits generated from **1** were undertaken to identify the resultant phases formed. Figure 3 shows the XRD plot of the various changes observed during the deposition at the different temperatures. In general, both the oxides of Sn (SnO_x = SnO, Sn_2O_3, Sn_3O_4) and Sn^0 were observed in the majority of films but the ratio of the phases present changed dramatically with temperature. Complete characterization of the individual phases was not undertaken for the individual SnO_x phases formed due to the complexity of the XRD patterns, the variety

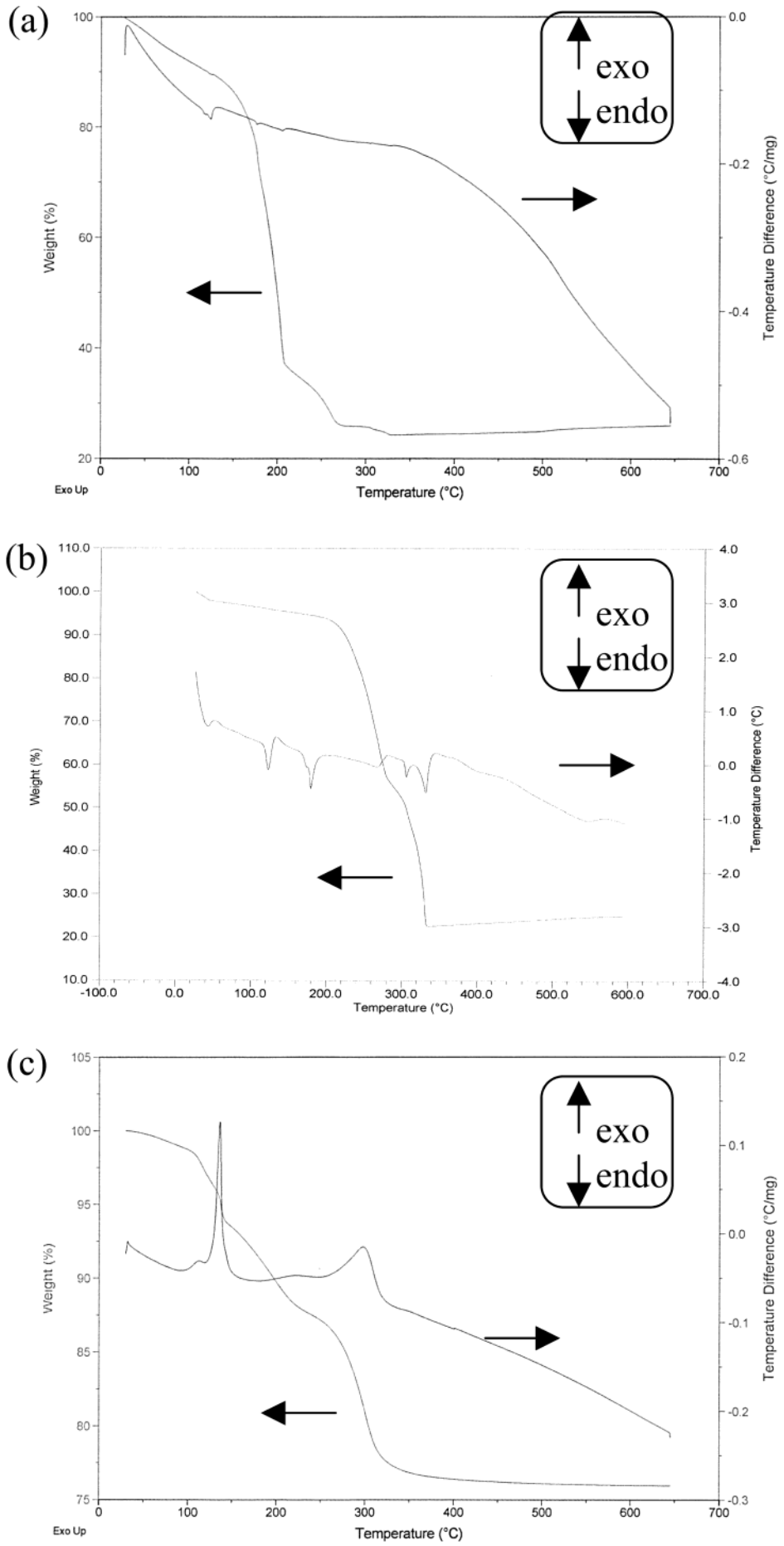

Figure 2. TGA/DTA of (a) **1**, (b) **2**, and (c) **3** under an atmosphere of argon 10 °C/min from room temperature to 650 °C.

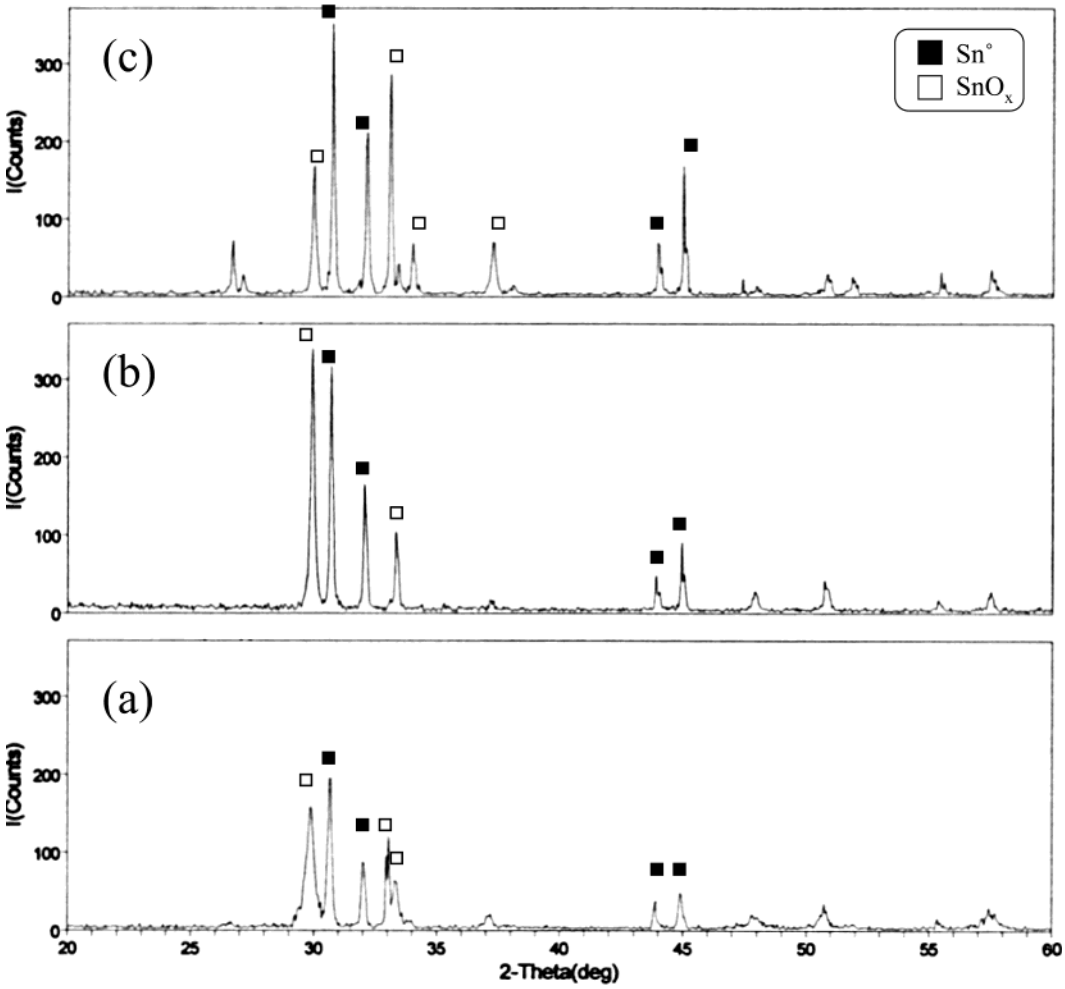

Figure 3. XRD of deposits of **1** at (a) 315, (b) 350, and (c) 450 °C.

of oxides formed, and the lack of additional information that would be garnered from this characterization effort. At the lower temperatures, tin oxides were present in roughly equal quantities with Sn^0; however, at higher temperatures (>350 °C) relatively greater amounts of Sn^0 were indicated by XRD.

To further characterize these films, SEM micrographs were obtained on each sample. Figure 4 shows the SEM micrograph of the various changes observed during the deposition at different temperatures. Deposits at 315 °C possessed a feathery and apparently faceted morphology. A side view revealed that this was not a continuous uniform film, but was in fact the deposition of crystalline particulate material on the substrate. As the temperature increased, the amount of deposited material decreased and eventually disappeared at ≈330 °C. As the temperature was further increased (>340 °C), a new morphology was observed as spherical particles. These particles increased in uniformity as the temperature increased but they decreased in size. This phenomenon was maintained until 470 °C, the maximum temperature investigated. EDS of the spherical particles conducted in the TEM indicated that these were Sn^0 spheres (Figure 5) possessing a surface layer of tin oxide.

Compound 2. XRD plots of the deposits obtained at different temperatures are shown in Figure 6. At low temperatures (330−350 °C), Sn^0 was observed as the dominant species present in the XRD plot (Figure 6a). As the temperature was increased, the oxides became more dominant, but significant amounts of Sn^0 were still present (Figure 6b). At high temperatures (>450 °C), XRD revealed predominantly Sn^0 with a small amount of oxide present (Figure 6c).

Figure 7 shows SEM micrographs of the resultant deposits at different temperatures. Gray powder deposits began at 330 °C and continued past 500 °C. Submicrometer-sized spheres of Sn^0 are present for the low-temperature (≈330 °C) deposits. As the temperature increased, surprisingly, wires and spheres were observed. At the end of each wire, a seed particle was easily observed. The wires were submicrometer in width but varied from several micrometers to tens of micrometers in length. The number of wires was found to decrease and the number of spheres increased, as the temperature was increased. TEM analysis indicated that the wires were SnO_x, apparently growing from a Sn^0 seed (Figure 8). Sn^0 seed particles were typically spherical and had a thin surface layer of tin oxide. Wire deposition was observed up to 450 °C whereupon a new morphology was observed. Above 450 °C, spherical particles were again observed. These spherical particles were significantly larger than the particles deposited at lower temperatures, ranging in size from a few micrometers to tens of micrometers.

Compound 3. The XRD spectra of the deposits from **3** had a comparatively small signal-to-noise ratio. In general, however, both the oxides and Sn^0 were observed

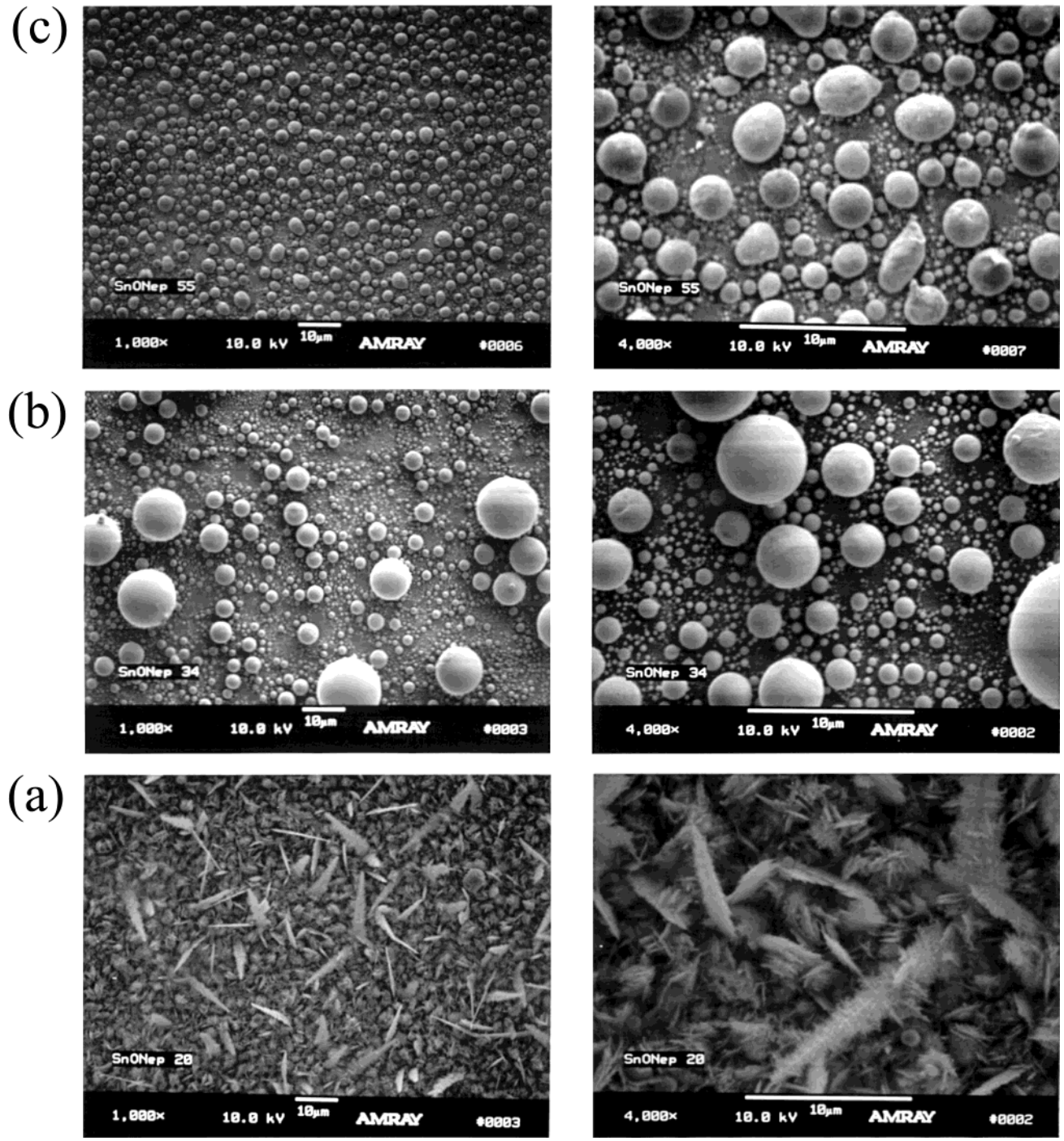

Figure 4. SEM of deposits of **1** at various temperatures: (a) 315, (b) 390, and (c) 470 °C.

in the majority of films but the ratio changed with temperature. Figure 9 shows the XRD spectra obtained for **3** over the temperatures of interest. At the lowest temperatures investigated, the oxides were present in roughly equal proportions with Sn^0. At intermediate temperatures in the vicinity of 380 °C, the pattern looks very similar to that of **2** at that temperature, except for a very strong oxide peak at $2\theta = 33°$, a phase that developed significantly only at higher deposition temperature with the other two compounds (note: this peak may also contain contributions from the Si(100) substrate). At high temperatures, increased Sn^0 was seen with **3**, similar to the trends observed with the other two compounds.

Figure 10 shows the SEM micrographs of the various changes observed during the deposition at different temperatures. Deposition of a gray powder on the substrate began at 350 °C and continued until 440 °C, the highest temperature investigated. At low temperatures, a mixture of spheres, platelets, and fiberlike particles were formed. At the intermediate temperature of 390 °C, platelet and fiberlike grains were organized into "fuzzy" spheres. As the temperature was further increased, the fuzzy material was more uniformly distributed and possessed an intricate lattice-like microstructure. TEM analysis revealed that these deposits are a mixture of SnO_x wires and ribbons, along with Sn^0 spheres at all deposition temperatures, though the

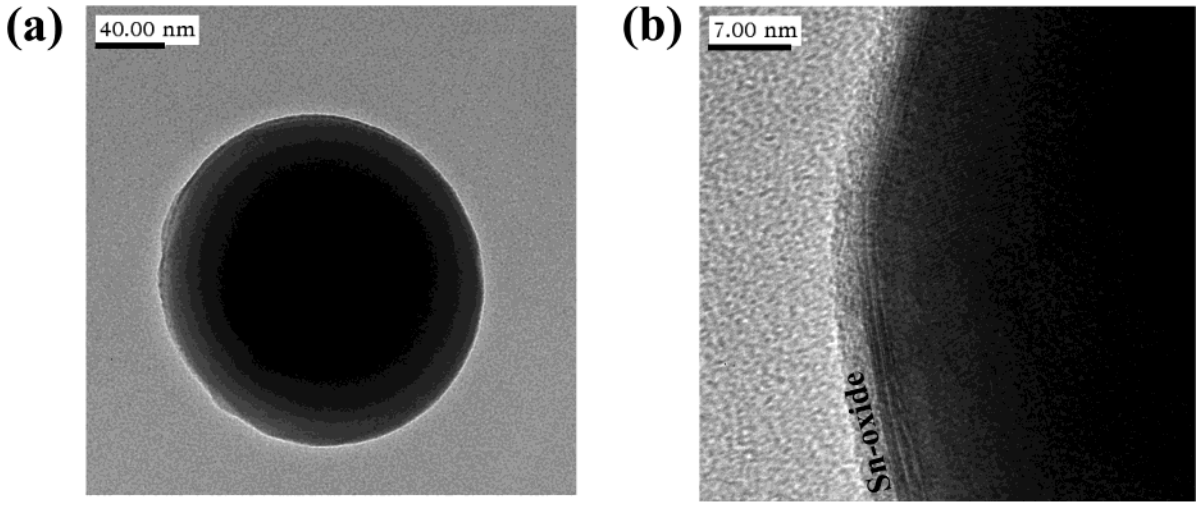

Figure 5. TEM of components of deposits from **1** deposited at 410 °C.

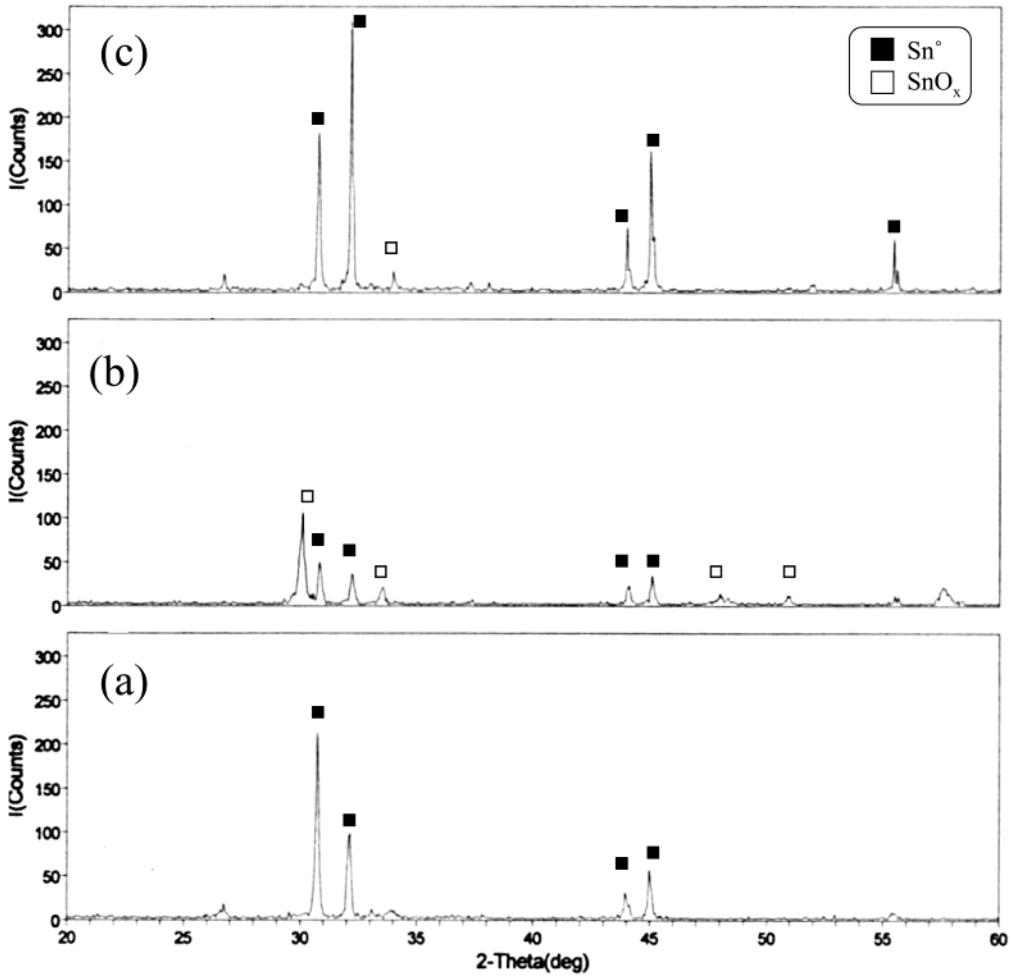

Figure 6. XRD of deposits of **2** at (a) 330, (b) 380, and (c) 500 °C.

number and size of Sn^0 depended on temperature. Figure 11 shows TEM micrographs that are representative of deposits with mixed fibers or ribbons and metal spheres. In most cases, a small Sn seed particle can be seen associated with each wire or ribbon, though larger Sn^0 particles are also seen that are not apparently associated with specific oxide growths. EDS revealed an oxide layer on Sn^0 particles that could be indexed to cassiterite in some instances (Figure 11c).

Discussion

For **1**−**3**, the thermal decomposition data indicate that these compounds would be suitable for MOCVD applications. The low melting points of these compounds combined with the more than expected weight loss of **1** and **2** in their TGA/DTA spectra are excellent indicators that these compounds can readily be transported to the gas phase without loss of structural integrity based on

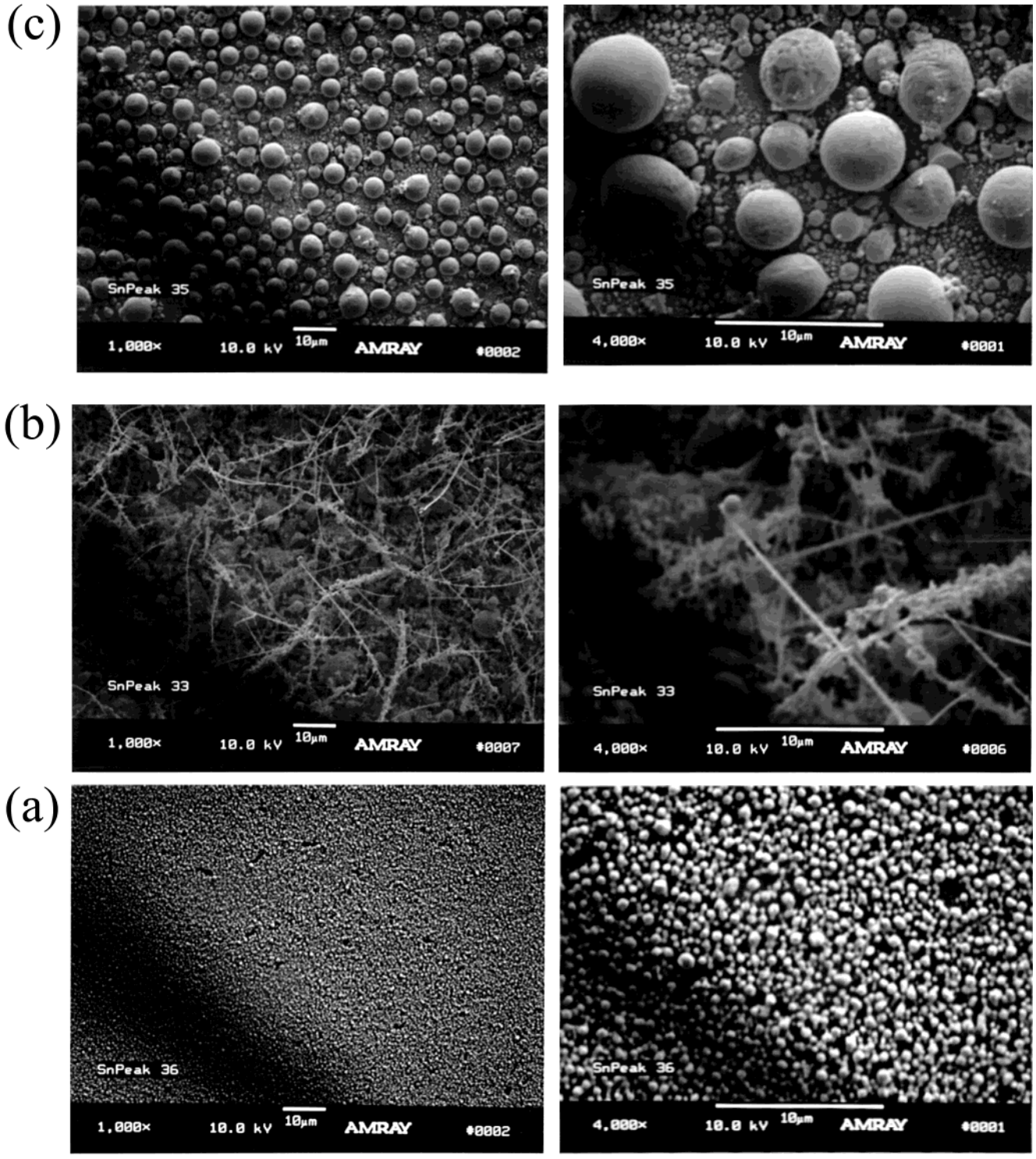

Figure 7. SEM of deposits of **2** at various temperatures: (a) 330, (b) 420, and (c) 500 °C.

the sublimation results. Further, the TGA/DTA data suggest that these compounds will decompose in an attractive temperature range. Interestingly, **2** displays the potential for rearrangement upon heating, as indicated by the presence of two melts in the TGA/DTA. Analytical data (including ^{119}Sn NMR, IR, and single-crystal analysis) of thermally treated **2** indicates that upon heating **2** is converted to **3**, which is not surprising based on the ready conversion through hydrolysis.

After these compounds were processed, the general trend of higher temperatures leading to more Sn^0 materials being deposited was noted. The disproportionation of the Sn(II) precursor to Sn(IV) oxides and Sn^0 may account for some of the lower combinations of oxide/metal materials. As the temperature increases, the reduction predominates. This trend is readily observed for **1** and **3**; however, **2** undergoes some anomalous behavior. On the basis of the thermal conversions noted above, when **2** is used as a MOCVD precursor, the precursor actually transforms into a mixture of **2** and **3**. Compound **3** forms deposits of mostly SnO_x when the substrate temperature is between 350 °C and 440 °C. Within this range, **2** deposited a more equal mixture of Sn^0 and SnO_x. Outside this range, **2** formed a deposit

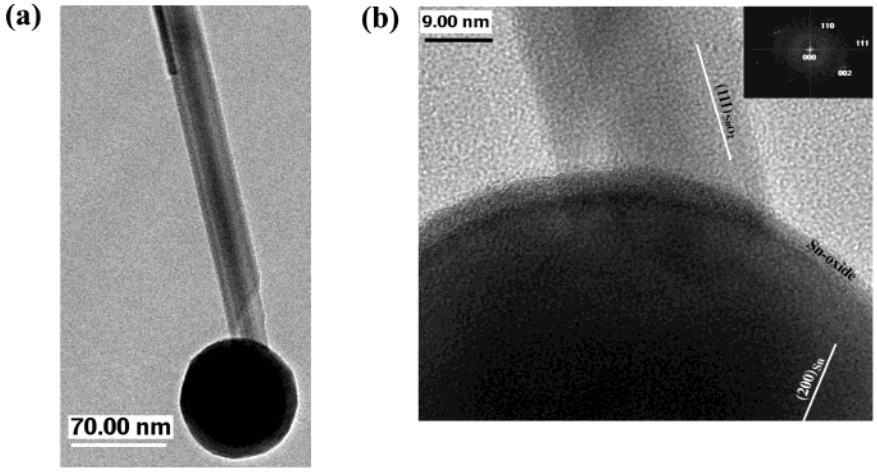

Figure 8. HRTEM of components of deposits from **2** deposited at 380 °C: (a) single SnO_2 rod and Sn^0 sphere and (b) higher magnification of the interface between the SnO_2 rod and metal sphere, also showing a thin layer of Sn oxide on the metal sphere surface. The insert is a fast Fourier transform (FFT) from the SnO_2 fiber, and the (200) lattice fringes of Sn^0 and (111) lattice fringes of SnO_2 (cassiterite) are also labeled.

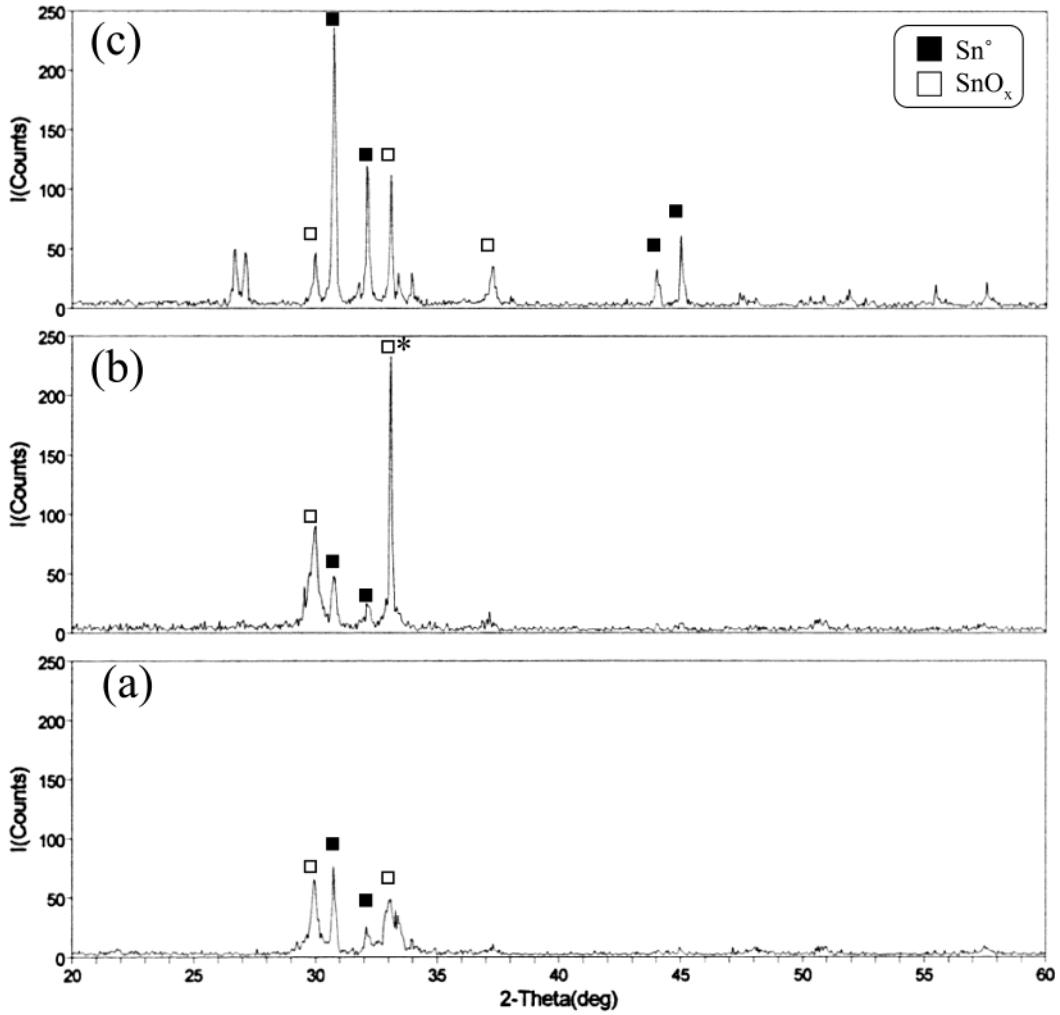

Figure 9. XRD of deposits of **3** at (a) 350, (b) 380, and (c) 440 °C.

of mostly Sn^0. To verify that **2** may undergo partial transformation to **3** under typical vaporization conditions, a sample of **2** was heated to 160 °C for 5 min under an argon atmosphere. FTIR and NMR analysis of that sample showed that it contained a mixture of **2** and **3**. Another sample of **2** was placed in the MOCVD reactor and was allowed to remain in the reactor at operational temperatures for an additional 5 min prior to opening the valve to the reactor. SEM analysis of the resultant deposits showed a morphology nearly identical to that of a deposit created by **3** at the same substrate temperature.

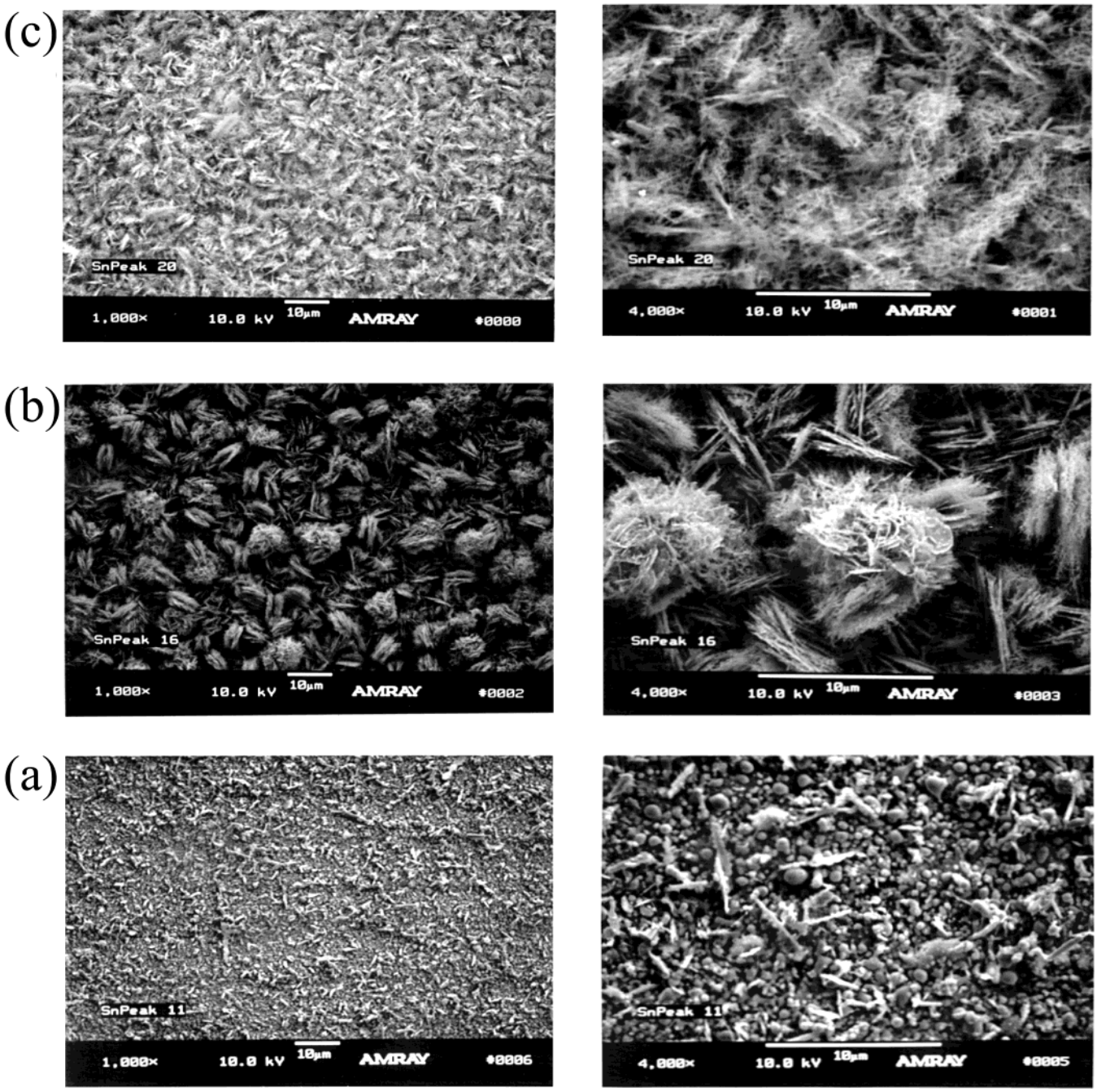

Figure 10. SEM of deposits of **3** at various temperatures: (a) 340, (b) 390, and (c) 430 °C.

It is of note that other alkoxide systems required the introduction of water or a significant O_2 partial pressure to successfully generate a thin film.[22] Under our "dry" conditions we were not able to generate a uniform thin film though deposition occurred. The three major deposit types observed here consisted of crystalline oxide flakes or particles, crystalline oxide fibers, and spherical metallic particles. The crystalline particles were very weakly adhered to the surface; thus, deposits were apparently initiated by particles deposited from the gas phase, with subsequent growth by CVD. The fibers and wires apparently form by the vapor−liquid−solid (VLS) growth mechanism[26] or a similar catalytic mechanism involving a liquid alloy droplet.[27] These growth mechanisms are enabled by the formation of Sn^0 and Sn(IV) via disproportionation of the Sn(II) precursor. Since the melting point of Sn^0 is 232 °C, Sn^0 formed in our experiments should be present as molten spheres during deposition. We believe that SnO_x dissolves into Sn^0 and crystallizes out of the metal melt at a particular location, growing the fiber from the base. Through the disproportionation mechanism, one reduced species (i.e., Sn°) should be generated for each oxidized cation (i.e., Sn(IV)) produced. Therefore, one should strictly expect the fiber volume to roughly match the metal sphere volume (appropriately scaled for density) that was visually observed in numerous micrographs. However, long thin fibers with a small metal sphere of about the same diameter as the fiber are also observed under

(26) Wagner, R. S.; Ellis, W. C. *Appl. Phys. Lett.* **1964**, *4*, 89.

(27) Hu, J.; Odom, T. W.; Lieber, C. M. *Acct. Chem. Res.* **1999**, *32*, 435.

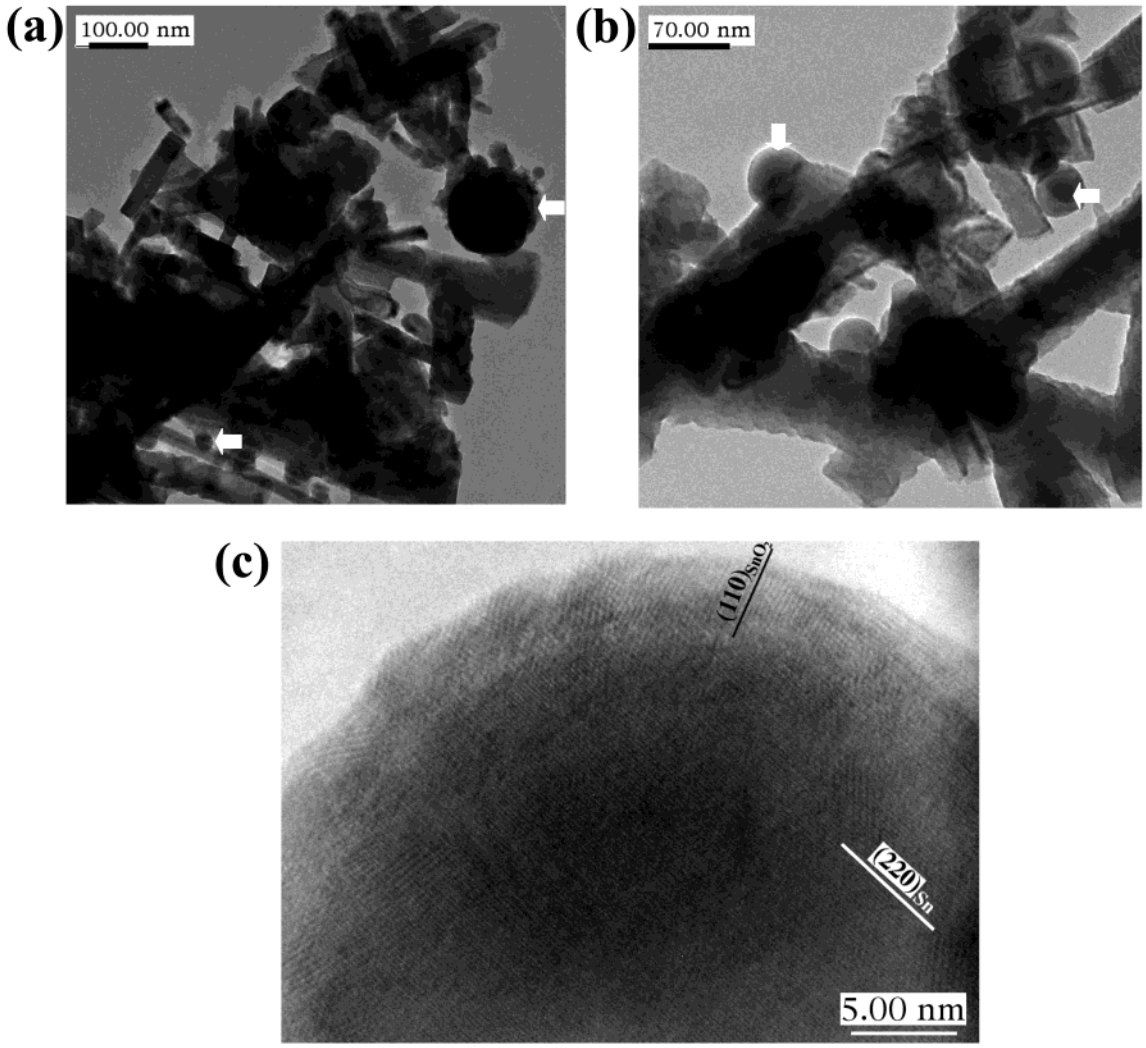

Figure 11. TEM of components of deposits from **3** deposited at 430 °C. The views are at different magnifications of (a) rods and sphere deposits, (b) alternative view of rods and spheres, and (c) a select sphere. Arrows indicate examples of select metal spheres within the sample matrix.

certain conditions. For these cases, the fiber may grow by CVD reactions from the tip after being initiated by the VLS mechanism, or the fiber may continue to grow by VLS, but with Sn(IV) being supplied directly to the molten metal from gas-phase species. The details of the mechanism are not completely clear, and some mix of disproportionation and direct CVD to the oxidized or reduced products probably accounts for the variety of morphologies observed and the variable Sn^0/SnO_x proportions at different deposition temperatures.

Summary and Conclusion

In this study, we have shown the utility of $[Sn(ONep)_2]_\infty$ (**1**), $[Sn_5(\mu_3{-}O)_2(\mu\text{-}ONep)_6]$ (**2**), and $[Sn_6(\mu\text{-}O)_4(ONep)_4]$ (**3**) as MOCVD precursors. The compounds all possess relatively low melting temperatures (below 190 °C) and acceptable volatility for direct vaporization. Compound **2** apparently undergoes partial decomposition to **3** under vaporization conditions, leading to potentially complex deposition behavior. However, **2** deposited at intermediate temperatures (≈380 °C) provided the highest loading of tin oxide wires observed. XRD analyses indicated that at low substrate temperatures the oxides were favored but at higher temperatures Sn^0 spheres were generated. While uniform films were not generated from these precursors, controlled depositions of tin oxide wires and ribbons mixed with Sn^0 particles were demonstrated wherein the oxide−metal phase content was controlled by the deposition temperature and the size of Sn^0 spheres controlled by the deposition temperature. Using these precursors to generate select morphological properties, we are undertaking the construction of complex devices (i.e., field emitters) using only MOCVD processes.

Acknowledgment. For support of this research, the authors would like to thank the Division of Materials Science and Engineering, Office of Science, U.S. Department of Energy, and the U.S. Department of Energy under Contract DE-AC04-94AL85000. Sandia is a multiprogram laboratory operated by Sandia Corporation, a Lockheed Martin Company, for the U.S. Department of Energy.

CM020893P